1521-009X/52/4/312–321$35.00
DRUG METABOLISM AND DISPOSITION

dx.doi.org/10.1124/dmd.123.001625
Drug Metab Dispos 52:312–321, April 2024

Interaction and Transport of Benzalkonium Chlorides by the Organic Cation and Multidrug and Toxin Extrusion Transporters

Letícia Salvador Vieira, Ryan P. Seguin, Libin Xu, and Joanne Wang

Department of Pharmaceutics (L.S.V., J.W.), Department of Medicinal Chemistry (R.P.S., L.X.), and Department of Environmental and Occupational Health Sciences, School of Public Health (L.X.), University of Washington, Seattle, Washington

Received December 8, 2023; accepted January 29, 2024

ABSTRACT

Humans are chronically exposed to benzalkonium chlorides (BACs) from environmental sources. The U.S. Food and Drug Administration (FDA) has recently called for additional BAC safety data, as these compounds are cytotoxic and have great potential for biochemical interactions. Biodistribution studies revealed that BACs extensively distribute to many tissues and accumulate at high levels, especially in the kidneys, but the underlying mechanisms are unclear. In this study, we characterized the interactions of BACs of varying alkyl chain length (C8 to C14) with the human organic cation transporters (hOCT1–3) and multidrug and toxin extrusion proteins (hMATE1/2K) with the goal to identify transporters that could be involved in BAC disposition. Using transporter-expressing cell lines, we showed that all BACs are inhibitors of hOCT1–3 and hMATE1/2K (IC_{50} ranging 0.83–25.8 μM). Further, the short-chain BACs (C8 and C10) were identified as substrates of these transporters. Interestingly, although BAC C8 displayed typical Michaelis-Menten kinetics, C10 demonstrated a more complex substrate-inhibition profile. Transwell studies with transfected Madin-Darby canine kidney cells revealed that intracellular accumulation of basally applied BAC C8 and C10 was substantially higher (8.2- and 3.7-fold, respectively) in hOCT2/hMATE1 double-transfected cells in comparison with vector-transfected cells, supporting a role of these transporters in mediating renal accumulation of these compounds in vivo. Together, our results suggest that BACs interact with hOCT1–3 and hMATE1/2K as both inhibitors and substrates and that these transporters may play important roles in tissue-specific accumulation and potential toxicity of short-chain BACs. Our findings have important implications for understanding human exposure and susceptibility to BACs due to environmental exposure.

SIGNIFICANCE STATEMENT

Humans are systemically exposed to benzalkonium chlorides (BACs). These compounds broadly distribute through tissues, and their safety has been questioned by the FDA. Our results demonstrate that hOCT2 and hMATE1 contribute to the renal accumulation of BAC C8 and C10 and that hOCT1 and hOCT3 may be involved in the tissue distribution of these compounds. These findings can improve our understanding of BAC disposition and toxicology in humans, as their accumulation could lead to biochemical interactions and deleterious effects.

Introduction

Benzalkonium chlorides (BACs) are quaternary ammonium compounds (Fig. 1) with alkyl chain lengths ranging from 8 to 18 carbons (C8 to C18). These compounds are cationic surfactants with broad antimicrobial properties and are widely used as disinfectants or preservatives in cleaning products, in medical products, and in the food processing industry (Pereira and Tagkopoulos, 2019). Although BACs have been used in consumer products since the 1950s and were believed to be safe, a broad spectrum of cytotoxic effects has been reported in various biologic systems (Herman and Bass, 1989; Nałecz-Jawecki et al., 2003; Sarkar et al., 2012; Melin et al., 2014; Hrubec et al., 2017; Herron et al., 2021; Arnold et al., 2023), and the US Food and Drug Administration (FDA) has called for further safety data concerning its use in healthcare and consumer antiseptic products (US FDA, 2015, 2016).

The widespread use of cleaning products containing BACs in hospitals, in restaurants, and at home indicates that humans are frequently and chronically exposed to these compounds. Indeed, a study analyzing human serum samples collected before (n = 111) and during (n = 111) the COVID-19 pandemic detected BACs in more than 95% of samples and showed a 174% increase in the median BAC concentration during the pandemic when compared with prepandemic levels (Zheng et al., 2021). Moreover, another study found that the blood concentrations of BACs correlated with toxicological endpoints such as decreased mitochondrial function, increased inflammatory cytokines, and altered sterol biosynthesis (Hrubec et al., 2021). Importantly, short-chain BACs were found to be highly potent inhibitors of cholesterol biosynthesis in cell lines (Herron et al., 2016), suggesting that even low levels of BAC exposure could lead to significant biochemical interactions.

Biodistribution studies in rats have reported that after oral or intravenous administration, BACs are highly distributed to several tissues, including the heart, liver, lungs, spleen, and kidneys (Xue et al., 2002, 2004; Kera et al., 2021). The kidney was identified as a major organ of

This work was financially supported by grants from National Institutes of Health National Institute of Environmental Health Sciences [Grant R01ES031927] (to L.X.) and National Institute of General Medical Sciences [Grant R01GM066233] (to J.W.). The content is solely the responsibility of the authors and does not necessarily represent the official views of National Institutes of Health.

The authors declare that they have no conflicts of interest with the contents of this article.

dx.doi.org/10.1124/dmd.123.001625.

This article has supplemental material available at dmd.aspetjournals.org.

ABBREVIATIONS: BAC, benzalkonium chloride; BCA, bicinchoninic acid; HEK, human embryonic kidney; hMATE, human multidrug and toxin extrusion protein; hOCT, human organic cation transporter; K_m, Michaelis-Menten constant; KRH, Krebs-Ringer-HEPES; LC-MS/MS, liquid chromatography tandem mass spectrometry; MDCK, Madin-Darby canine kidney; P_{app}, apparent permeability.

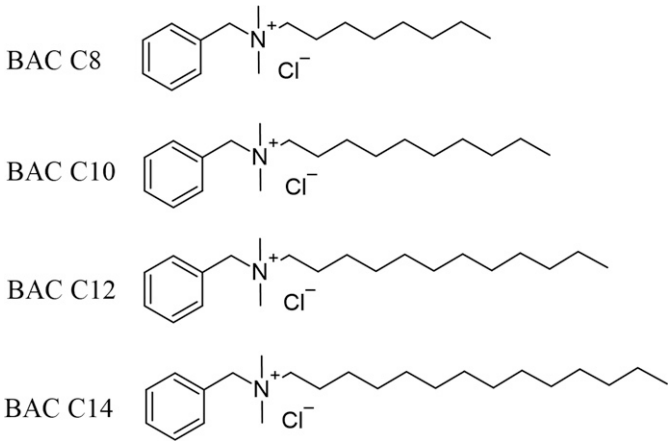

Fig. 1. Structure of benzalkonium chlorides (BAC) C8, C10, C12, and C14.

accumulation, showing a preferential accumulation of shorter-chain BACs (Kera et al., 2021). Additionally, BAC C12 and C16 have been reported to cross the blood-placental barrier and to reach mouse neonatal brains (Herron et al., 2019). Although tissue distribution in humans is more difficult to assess, pathologic examinations after poisoning cases reported lungs, heart, liver, and kidneys as affected tissues (van Berkel and de Wolff, 1988; Hitosugi et al., 1998; Tambuzzi et al., 2022). In particular, a case report of delayed death after suicidal ingestion of Lysoform—containing BACs as the main constituent—showed clear signs of acute kidney injury, including foci of tubular necrosis (Tambuzzi et al., 2022). These emerging evidences demonstrate that BACs distribute and accumulate in various human tissues with potential toxicological effects. However, the mechanisms driving the accumulation of BACs in these tissues are poorly understood.

The human polyspecific organic cation transporters are a group of solute carrier transporters that mediate cellular transport of many endogenous and exogenous organic cations, impacting their systemic and tissue-specific disposition (Giacomini et al., 2010; Wagner et al., 2016; Koepsell, 2020). This group includes the organic cation transporters 1, 2, and 3 (hOCT1, hOCT2, and hOCT3) and the multidrug and toxin extrusion proteins 1 and 2K (hMATE1 and hMATE2K). Interestingly, the tissue distribution of these transporters largely overlaps with tissues in which BAC accumulation has been reported (Kera et al., 2021). For instance, hOCT1 is a major isoform highly expressed in the liver known to mediate uptake of organic cations into hepatocytes; hOCT2 and hMATE1/2K are expressed respectively in the basal and apical membranes of renal proximal tubule cells and facilitate renal uptake and tubular secretion of its substrates; and hOCT3 is broadly expressed in several tissues, including the heart, skeletal muscle, and placenta, playing a significant role in drug transport in these organs (Wagner et al., 2016; Lee et al., 2018). We thus hypothesized that hOCTs and hMATEs are transporters involved in the disposition of BACs.

Although hOCTs and hMATEs have been previously reported to interact with various quaternary ammonium compounds (Zhang et al., 1999; Dresser et al., 2002; Tanihara et al., 2007; Sala-Rabanal et al., 2013), their interaction with BACs has never been investigated. In this study, we characterized the interactions of BACs of varying alkyl chain lengths with hOCT1–3 and hMATE1/2K transporters. Compounds were investigated as potential inhibitors and substrates, and detailed kinetic interactions were characterized. The potential impact of hOCT2 and hMATE1 in BAC renal disposition was investigated using an in vitro model of renal transepithelial transport employing hOCT2/hMATE1 double-transfected cells.

Materials and Methods

Materials. [^{14}C]metformin (115 mCi/mmol) was purchased from Moravek Biochemicals, Inc. (Brea, CA). Optima liquid chromatography-mass spectrometry (LC-MS)–grade acetonitrile, water, formic acid, and ammonium formate used in liquid chromatography were purchased from Fisher Scientific (Santa Clara, CA). Lucifer yellow (LY) was from MP Biomedicals (Irvine, CA). Benzalkonium chlorides (BACs) of various alkyl chain lengths (C8, C10, C12, and C14) were from Sigma-Aldrich (St. Louis, MO). Deuterated (d7-benzyl) BACs (d_7-C10-BAC, d_7-C12-BAC, and d_7-C14-BAC) were synthesized as previously described (Herron et al., 2016). Cell culture media and reagents were purchased from Invitrogen (Carlsbad, CA).

Cell Lines and Cell Culture. Flp-In human embryonic kidney (HEK)293 cells stably transfected with hOCT1–3, hMATE1, hMATE2K, or empty pcDNA5/FRT vector (control) were previously established in our laboratory (Duan and Wang, 2010; Yin et al., 2015). HEK293 cells were cultured in high-glucose Dulbecco's modified Eagle's medium supplemented with 10% fetal bovine serum, 2 mM L-glutamine, 100 IU/ml penicillin, 100 μg/ml streptomycin, and 150 μg/ml hygromycin B. The flasks and plates used were coated with 0.1 mg/ml poly-D-lysine in Milli-Q water to improve the attachment of the HEK293 cells. The Madin-Darby canine kidney (MDCK) cells double transfected with hOCT2 and hMATE1 or empty vector were previously generated and validated in our laboratory (Yin et al., 2015). These cells were maintained in high-glucose Dulbecco's modified Eagle's medium supplemented with 15% fetal bovine serum, 500 μg/ml G418, and 200 μg/ml hygromycin B. All cell lines were cultured in a 37°C humidified incubator with 5% CO_2.

Uptake and Inhibition Assays in HEK293 Cells. Uptake and inhibition assays were performed as previously described (Duan and Wang, 2010; Yin et al., 2015, 2016) with modifications for analysis of BACs by liquid chromatography tandem mass spectrometry (LC-MS/MS). Briefly, HEK293 cells were seeded in 96-well plates and grown to greater than 90% confluency (1 to 2 days). Prior to incubation, cells were washed twice with prewarmed Krebs-Ringer-HEPES (KRH) buffer (5.6 mM glucose, 125 mM NaCl, 4.8 mM KCl, 1.2 mM KH2PO4, 1.2 mM CaCl2, 1.2 mM MgSO4, and 25 mM HEPES, pH 7.4). Uptake was initiated by the addition of buffer at 37°C containing a substrate with or without inhibitor. For hOCT-transfected cells KRH at pH 7.4 was used, whereas for hMATE-transfected cells KRH was adjusted to pH 8.0. Uptake was quenched by washing the cells three times with ice-cold KRH buffer. After washing, cells from incubations with BACs were permeabilized with 100 μl acetonitrile:water (1:1) containing 50 nM internal standard (d_7-BACs) for analysis by LC-MS/MS. Precipitated protein was then solubilized in 100 μl 1 M NaOH at 37°C for 1 hour and neutralized with 100 μl 1 M HCl, and protein content from each well was measured by the bicinchoninic acid (BCA) method. For incubations containing radiolabeled substrate (^{14}C-metfomin), cells were directly lysed with 1 M NaOH and neutralized with 1 M HCl, and the lysate was used for protein quantification (BCA method) and for measuring radioactivity by liquid scintillation counting (Tri-Carb, Perkin Elmer, Waltham, MA). For inhibition studies,^{14}C-metformin was used as the classic substrate at 8.7 μM (1 μCi/ml), well below its reported Michaelis-Menten constant (K_m) value for these transporters (Liang and Giacomini, 2017). Experiments were performed within the initial rate period. Transporter-specific uptake was determined by subtracting the uptake observed in the control (pcDNA5 vector-transfected) cells. Additionally, uptake in the presence of inhibitor was normalized relative to the uptake observed in the absence of inhibitor.

Trans-Stimulation Studies in HEK293 Cells. In trans-stimulation experiments, pcDNA5 (vector)-transfected and hOCT1-, hOCT2-, and hOCT3-transfected cells were preincubated for 15 minutes with KRH buffer at pH 7.4 with or without (control) 1 μM of indicated BAC. Cells were then rinsed two times with ice-cold KRH buffer before incubation at 37°C for 4 minutes in KRH buffer (pH 7.4) containing 8.7 μM (1 μCi/ml) ^{14}C-metformin. Cells were then rinsed three times with ice-cold KRH buffer and lysed with 1 M NaOH as described above. Radioactivity and protein content were measured in the lysate. Uptake in the vector-transfected cells was subtracted from transporter-transfected cells to obtain transporter-specific uptake, and metformin uptake after preincubation with BACs was normalized to uptake in the control condition.

Transwell Studies in hOCT2/hMATE1 Double-Transfected MDCK Cells. Transepithelial flux of BACs across MDCK cell monolayers was determined as previously described with slight modifications (Yin et al., 2015, 2016;

López Quiñones et al., 2020). Briefly, empty vector and hOCT2/hMATE1-expressing MDCK cells were seeded at a density of 2×10^5 cells/cm^2 on 12-well Corning Transwell inserts (PET membrane, 0.4 μm pore size). Transport experiments were performed 5 days after seeding. These studies were performed under a pH gradient (basolateral pH 7.4 and apical pH 6.0). The apical pH of 6.0 was chosen based on previously published methods by our and other laboratories to mimic the average urine pH (Tsuda et al., 2009; Rowland and Tozer, 2010; Müller et al., 2011; Yin et al., 2015). Measurement of transepithelial flux of lucifer yellow (50 μM) was used to verify the integrity of the MDCK monolayer and the formation of tight junctions. Only data from inserts with less than 5% lucifer yellow transfer over the 2-hour time course were accepted [apparent permeability (P_{app}) < 1.6×10^{-6} cm/s]. After removal of cell culture media from both sides of the inserts, cells were carefully washed three times with warm KRH buffer pH 7.4. For apical-to-basal (A-to-B) transport, 1.5 ml KRH buffer (pH 7.4) was added to the B chamber, and transport was initiated by adding 0.5 ml KRH (pH 6.0) containing 1μM BAC (C8 or C10) and lucifer yellow (50 μM) to the A chamber. Similarly, for basal-to-apical (B-to-A) transport, 0.5 ml KRH buffer (pH 6.0) was added to the A chamber, and transport was initiated by adding 1.5 ml KRH (pH 7.4) containing BAC and lucifer yellow to the B chamber. When pyrimethamine was used, it was added to the A chamber only at 10 μM. To measure transcellular transport, at each time point, 100 μl was collected from the receiving chamber and replaced with the adequate buffer. Fluorescence measurements of lucifer yellow were performed from a top-read position in a Synergy HTX plate reader (BioTek, Winooski, VT) using a 420/50-nm excitation and 528/20-nm emission filter set. After fluorescence was measured, 100 μl acetonitrile containing 100 nM d_7-BACs was added to each sample, followed by centrifugation and quantification of BACs by LC-MS/MS. At the final time point (120 minutes), the inserts were washed three times with ice-cold KRH buffer, and cells were permeabilized using acetonitrile containing 100 nM d_7-BACs, diluted 1:1 with KRH buffer and centrifuged before LC-MS/MS analysis. After permeabilization, the precipitated protein was solubilized with 1 M NaOH and neutralized with 1 M HCl, and protein content was measured by BCA method and used to normalize intracellular accumulation of BACs.

Quantification of BACs by LC-MS/MS. Levels of BAC C8, C10, C12, and C14 were quantified using an LC-MS/MS system consisting of a Waters ACQUITY UPLC system coupled to a Waters SYNAPT XS quadrupole time-of-flight (QToF) mass spectrometer (Waters Corporation, Milford, MA). Samples were prepared in 50% acetonitrile containing 50-nM individual d_7-BACs as internal standards. The autosampler compartment was maintained at 10°C from which 8-μl sample aliquots were injected to the LC column by a flow-through needle. Reversed-phase analyte separation was performed on a Thermo Hypersil GOLD C_{18} column (100 × 2.1 mm, 1.9 μm particle size) operated at ambient temperature and 0.4 ml/min flow rate. The initial mobile phase composition of solvent A (water with 0.1% formic acid and 2 mM ammonium formate) and solvent B (acetonitrile) was 80% A and 20% B. Percent B was linearly increased at a rate of 6% per minute out to 10 minutes to reach 80% B. Percent B then increased to 100% to wash the column for 2 minutes before returning to the initial conditions (20% B) to reequilibrate the column for 2 minutes prior to the next injection. Electrospray ionization in positive ion mode (ESI+) was run under the following source conditions: capillary voltage 2.5 kV, cone voltage 30 V, source offset 10 V, source temperature 150°C, desolvation temperature 500°C, cone gas flow 50 l/h, desolvation gas flow 1000 l/h, and nebulizer gas flow 6.5 bar. The mass detector underwent calibration using sodium formate cluster ions immediately prior to each run. Throughout data acquisition, leucine-enkephalin lock mass ($[M+H]^+$ 556.2771 *m/z*) was sampled at regular intervals and used as the reference for mass correction.

Targeted MS/MS detection of BACs was accomplished by isolation of the precursor $[M]^+$ ions in the quadrupole followed by fragmentation in the transfer cell and accurate mass measurement by the time-of-flight mass analyzer. Fragmentation of BAC $[M]^+$ precursor ions produced $[M - benzyl]^+$ and $[benzyl]^+$ as the two major fragment ions for the unlabeled BACs or $[M - d_7\text{-benzyl}]^+$ and $[d_7\text{-benzyl}]^+$ fragment ions for deuterium-labeled d_7-BAC internal standards. The precursor to product mass-to-charge (*m/z*) transitions monitored for each analyte are described in Supplemental Table 1. LC-MS/MS chromatograms were accurate mass filtered (±0.020 Da) for the two major fragment ions, and the resulting peak areas were integrated using TargetLynx application manager in MassLynx software (Waters Corporation). Analyte peak areas were normalized to the appropriate internal standard peak area. Specifically, d_7-BAC-C10 served as the internal standard for BAC-C8 and BAC-C10, d_7-BAC-C12 as the internal standard for BAC-C12, and d_7-BAC-C14 as the internal standard for BAC-C14.

Data Analysis. Inhibition, uptake, and trans-stimulation studies in HEK293 cells were performed in triplicate and repeated at least three independent times. BAC concentrations were corrected based on nonspecific binding to plastic, which was determined by comparison of drug concentration when diluted in organic solvent in comparison with KRH buffer. Transwell studies in MDCK cells were performed in one (A-to-B direction) or two (B-to-A direction) individual apparatuses and were repeated at least three times. Data are reported as mean ± S.D. Data were plotted and fitted through nonlinear regression using GraphPad Prism 7.0 (GraphPad Software Inc., La Jolla, CA). IC_{50} values were obtained by fitting the following four-parameter dose-dependent inhibition equation to the data:

$$v = Bottom + \frac{Top - Bottom}{1 + \left(\frac{[I]}{IC_{50}}\right)^H} \quad (1)$$

where v is the rate of uptake in the presence of inhibitor, "Bottom" is the residual noninhibitable baseline value, "Top" is the rate of uptake in the absence of inhibitor, [I] is the inhibitor concentration, and H is the Hill coefficient. To obtain graphs and kinetic parameters, the Michaelis-Menten equation was fitted by nonlinear regression to the BAC C8 data:

$$v = \frac{V_{max} * [S]}{K_m + [S]} \quad (2)$$

where v represents the uptake velocity, V_{max} denotes the maximum uptake velocity of the system, K_m is the Michaelis-Menten constant, and [S] indicates the substrate concentration. A substrate-inhibition kinetic model previously described (Leow and Chan, 2019) was fitted to the BAC C10 transporter-specific uptake data:

$$v = \frac{V_{max} * [S]}{K_m + [S] * \left(1 + \frac{[S]}{K_{i,[S]}}\right)} \quad (3)$$

where $K_{i,[S]}$ is the affinity constant for binding of the substrate to the inhibitory site. For the transwell experiments, the P_{app} of BAC C8 and C10 were calculated using the following equation:

$$P_{app} = \left(\frac{dQ}{dt}\right)/(A * C_o) \quad (4)$$

where dQ/dt represents the amount of compound transported over time, A is the surface area of the insert membrane, and C_0 is the initial compound concentration in the donor chamber. Statistical significance was assessed using one-way ANOVA followed by Dunnett's post hoc test to correct for multiple comparisons or an unpaired Student's *t* test (with or without Bonferroni post hoc test for multiple comparisons) as specified in the figure legends. A *P* value below 0.05 was deemed statistically significant.

Results

BACs Are Strong Inhibitors of the Polyspecific Organic Cation Transporters. To determine if BACs of varying alkyl chain lengths (C8, C10, C12, and C14) interact with hOCT1, 2, and 3 and hMATE1 and 2K, the uptake of the probe substrate metformin was measured in the absence and presence of varying BAC concentrations. Metformin was used at 8.7 μM, well below its reported K_m value for these transporters (Liang and Giacomini, 2017). All BACs inhibited metformin uptake by hOCT1–3 and hMATE1/2K, displaying dose-dependent inhibition with IC_{50} values ranging from 0.83 to 25.8 μM (Fig. 2; Table 1). To examine whether BAC chain length impacts inhibition potency, the IC_{50} values toward each transporter were plotted as a function of BAC chain length (Fig. 3). No apparent trend was observed. However, hMATE1 seems to be the most sensitive transporter to BACs with IC_{50} values consistently lower than other transporters (Fig. 3; Table 1). Interestingly, a stimulatory effect on hOCT2-mediated metformin uptake was observed for C8 and C10 at low concentrations (Fig. 2, A and B), which was not observed for C12 or C14 (Fig. 2, C and D). This stimulatory effect may be due to trans-stimulation of the transporter. We thus performed trans-stimulation

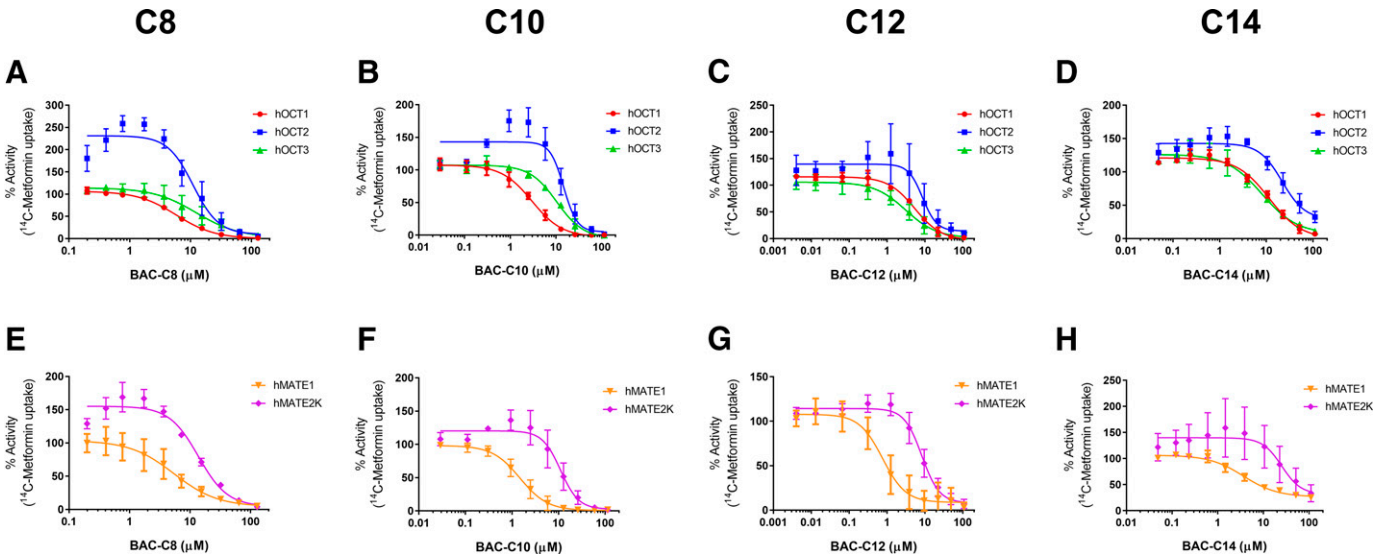

Fig. 2. Dose-dependent inhibition of hOCT1, hOCT2, hOCT3, hMATE1, and hMATE2K by BAC C8, C10, C12, and C14. Uptake of ^{14}C-metformin (8.7 μM) in the absence and presence of BAC C8 (A and E), C10 (B and F), C12 (C and G), and C14 (D and H) was measured in both vector- and transporter-transfected HEK293 cells for 4 minutes at 37°C. Transporter-specific uptake was obtained by subtracting the activity in vector cells from the activity in transporter-expressing cells, and data are presented as percentage of metformin uptake in the absence of BACs. Each data point represents mean ± S.D. from at least three independent experiments. IC_{50} values obtained from the dose-dependent inhibition curves are summarized in Table 1.

studies in hOCT1–3 transfected HEK293 cells. As shown in Supplemental Fig. 1, preloading hOCT2-transfected HEK293 cells with BAC C8 and C10, but not C12 and C14, led to an enhanced uptake of metformin. No stimulation was observed for hOCT1 or hOCT3; instead, a slight transinhibitory effect by C8 and/or C10 was observed (Supplemental Fig. 1).

BAC C8 and C10 Are Transported by hOCT1–3 and hMATE1/2K. To determine if BACs are substrates of polyspecific organic cation transporters, we directly measured BAC accumulation in vector- and transporter-transfected HEK293 cells. At a substrate concentration of 1 μM and incubation time of 10 minutes, C8 significantly accumulated in cells expressing hOCT1, 2, and 3 (~13- to 16-fold) and hMATE1/2K (3.4 and 8.3-fold, respectively) in comparison with pcDNA5 vector cells (Fig. 4). Similarly, C10 also had significantly higher (~2.3 to 3.3-fold) accumulation in transporter-transfected cell lines. In contrast, C12 only displayed a slight uptake (<1.5-fold) in hOCT1 and hMATE2K-transfected cells, and no significant accumulation was observed for C14. These results demonstrate that short-chain BACs (C8 and C10) are substrates for hOCT1–3 and hMATE1/2K whereas longer-chain BACs are poor or not substrates for these transporters.

Transport Kinetics of BAC C8 and C10 by hOCTs and hMATEs. The accurate determination of transporter kinetic parameters requires the selection of time points in the initial linear phase of uptake (i.e., initial uptake rates) (Brouwer et al., 2013). Therefore, the time course of C8 and C10 uptake by hOCT1, hOCT2, hOCT3, hMATE1, and hMATE2K was examined to determine the initial uptake rate. The data showed that uptake of C8 and C10 was higher in transporter-expressing cells at all time points tested, and substantial accumulation was achieved after 5- to 10-minute incubation in comparison with vector-transfected cells (Fig. 5). Uptake of C8 and C10 by hOCT1–3 was linear up to 7–10 minutes (Fig. 5, A and B), and their uptake by hMATE1/2K was linear up to 4–7 minutes (Fig. 5, C and D). Hence, concentration-dependent studies to determine kinetic parameters were conducted with a 4-minute incubation time for hOCT1–3 and a 2-minute incubation time for hMATE1/2K. Specific uptake was obtained by subtracting uptake in vector-transfected cells.

As shown in Fig. 6, the uptake of C8 mediated by hOCT1, hOCT2, hOCT3, hMATE1, and hMATE2K displayed saturable kinetics with typical Michaelis-Menten curves, as confirmed by the linear nature of the Eadie-Hofstee plots. The K_m and V_{max} values for each transporter, obtained through nonlinear regression fitting to eq. 2, are summarized in Table 2. The apparent affinities of the human polyspecific organic cation transporters for C8 are similar, ranging from 6 to 19 μM, which is consistent with their IC_{50} values (ranging from 5 to 14 μM, Table 1).

TABLE 1

IC_{50} of BAC C8, C10, C12, and C14 of metformin uptake by hOCT1–3 and hMATE1/2K

Data are presented as mean ± S.D. of the IC_{50} values from three or four independent experiments.

	IC_{50} ± S.D. (μM)				
BAC	hOCT1	hOCT2	hOCT3	hMATE1	hMATE2K
C8	5.9 ± 0.6	11.9 ± 5.3	12.2 ± 6.8	4.9 ± 2.2	14.0 ± 2.9
C10	3.0 ± 0.7	14.9 ± 3.4	10.7 ± 1.2	1.6 ± 0.7	10.8 ± 4.0
C12	5.5 ± 0.9	8.4 ± 4.9	3.3 ± 1.5	0.83 ± 0.38	8.3 ± 2.2
C14	11.6 ± 2.1	24.0 ± 11.5	8.6 ± 1.6	3.7 ± 1.3	25.8 ± 6.8

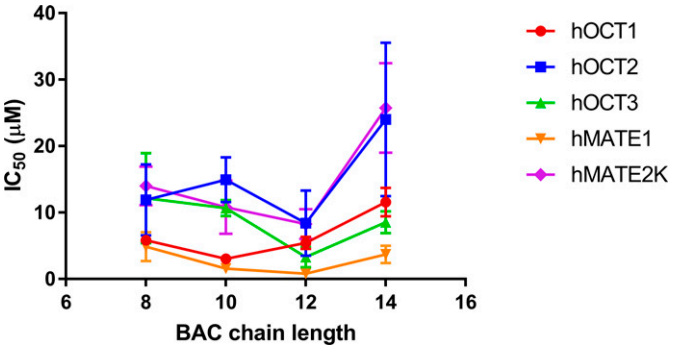

Fig. 3. Relationship between the alkyl chain length of BACs and their IC_{50} toward hOCT1, hOCT2, hOCT3, hMATE1, and hMATE2K. Each point represents the mean ± S.D. IC_{50} value obtained from at least three independent experiments. Although no apparent trend was observed between inhibitory potency and alkyl chain length, BACs appear to be slightly more potent inhibitors of hMATE1.

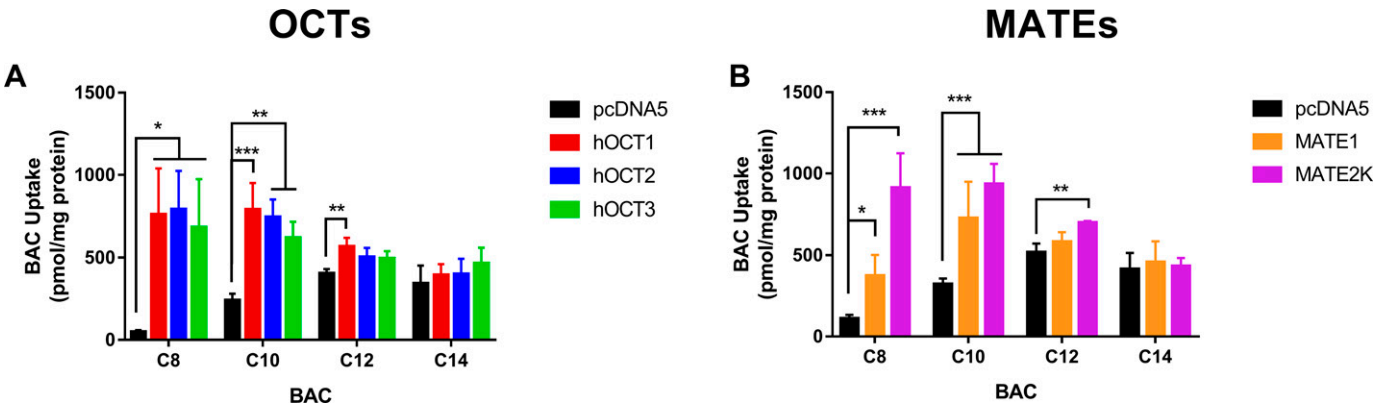

Fig. 4. Uptake of BAC C8, C10, C12, and C14 by hOCT1–3 (A) and hMATE1/2K (B). The uptake of 1 μM BAC (C8 to C14) was measured after 10-minute incubation at 37°C in both pcDNA5 (vector) and transporter-expressing HEK293 cells. Data are presented as the means ± S.D. from three independent experiments. The uptake of each BAC in transporter-expressing cells was compared with that in vector-transfected cells (*P < 0.05; **P < 0.01; ***P < 0.001). Statistical significance was determined by using one-way ANOVA followed by Dunnett's test.

Interestingly, C10 displayed an atypical transport kinetic profile for all hOCTs and hMATEs, with a hook in the upper left quadrant in the Eadie-Hofstee plot (Fig. 7). These patterns could suggest substrate inhibition kinetics due to substrate binding to multiple sites in these transporters where binding to a secondary site may hinder transport efficiency. We then fit C10 kinetics data to eq. 3, which includes an affinity constant for binding to the inhibitory site ($K_{i,[s]}$). The K_m, V_{max}, and $K_{i,[s]}$ values calculated for each transporter are presented in Table 2. The estimated $K_{i,[s]}$ values are 5- to 15-fold higher than the K_m for hOCT1, hOCT2, hMATE1, and hMATE2K, indicating a higher affinity to the binding site that results in substrate translocation. On the other hand, the K_m and $K_{i,[s]}$ for hOCT3 are more comparable, suggesting that the affinities to the translocation and the inhibition binding sites are less discernible.

Transepithelial Transport of BAC C8 and C10 in hOCT2/hMATE1-Transfected MDCK Cells. The hOCT2 and hMATE1/2K transporters work sequentially to mediate tubular secretion of their substrates, and how they function can influence intrarenal accumulation of compounds (Yin and Wang, 2016). Previous studies have revealed significant renal accumulation of BACs in rats after oral and intravenous dosing, with higher accumulation reported for shorter-chain BACs (Xue et al., 2004; Kera et al., 2021). Our uptake study in HEK293 transporter-transfected cells shows that BAC C8 and C10 are substrates of hOCT2 and hMATE1/2K (Figs. 4–5). To investigate the potential

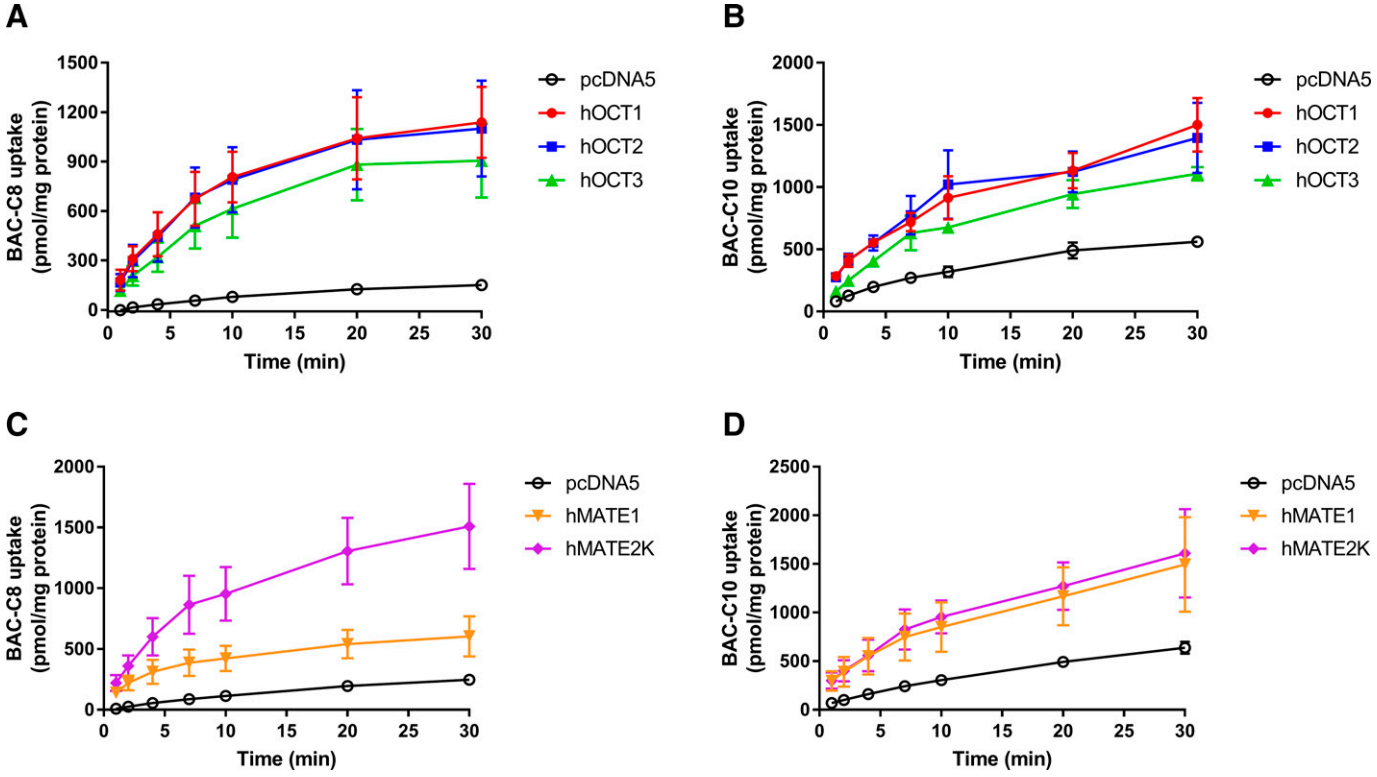

Fig. 5. Time course of uptake of BAC C8 and C10 uptake mediated by hOCT1–3 and hMATE1/2K. Uptake of 1 μM BAC C8 (A and C) or C10 (B and D) was measured in HEK293 cells expressing pcDNA5 empty vector (black), hOCT1 (red), hOCT2 (blue), hOCT3 (green), hMATE1 (orange), and hMATE2K (magenta) at specified time points (1 to 30 minutes) at 37°C. Data points represent the mean ± S.D. from three independent experiments.

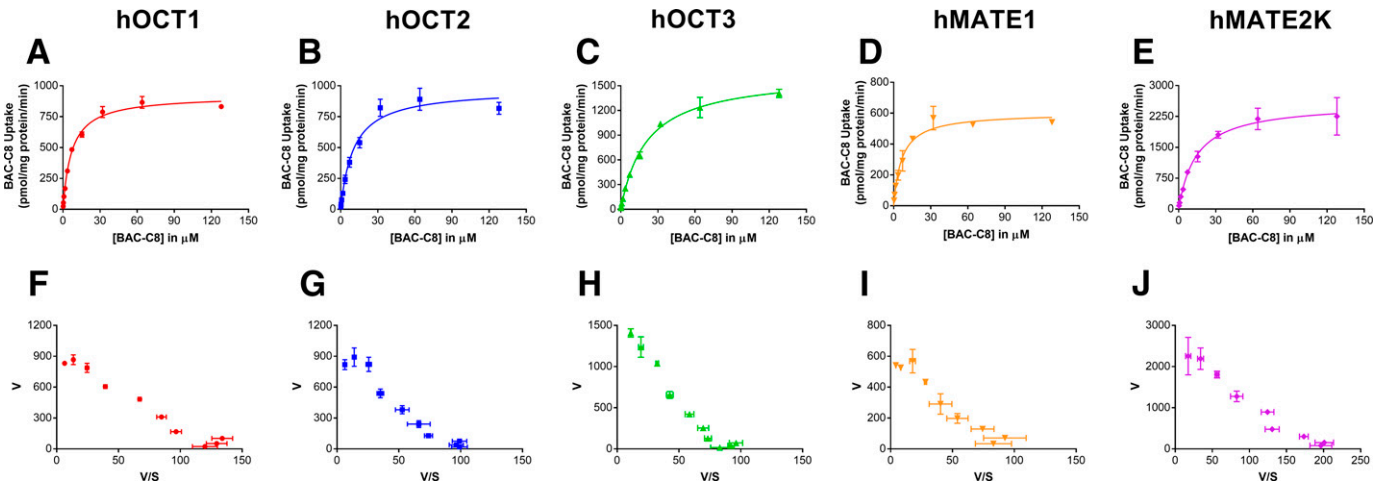

Fig. 6. BAC C8 uptake kinetics by hOCT1–3 and hMATE1/2K. Concentration-dependent uptake was measured in both control and transporter-expressing cell lines at 37°C within the linear phase of uptake (4 minutes for hOCT1–3 and 2 minutes for hMATE1/2K). Transporter-specific uptake was obtained by subtracting the uptake in control cells from the uptake in transporter-expressing cells. (A–E) panels display saturation curves and (F–J) panels show Eadie-Hofstee transformations for the kinetic data. Based on the Eadie-Hofstee plots, the standard Michaelis-Menten equation (eq. 2) was fitted to the data from hOCT1- (A), hOCT2- (B), hOCT3- (C), hMATE1- (D), and hMATE2K- (E) mediated uptake of BAC C8. Concentration-dependent uptake was performed independently three times for each transporter, and results from one representative experiment are shown. Data points represent the mean ± S.D. from one representative experiment in triplicate. The kinetic parameters summarized in Table 2 are the mean ± S.D. of the values from all three independent experiments.

role of these transporters in renal secretion and intrarenal accumulation of these compounds, transepithelial flux and accumulation of BAC C8 and C10 were assessed in a transwell system employing vector-transfected and hOCT2/hMATE1-double transfected MDCK cells. As shown in Fig. 8, A and B, the B-to-A flux rates of BAC C8 and C10 were constant over the 120-minute time course, and transport was higher in the double-transfected cells in comparison with vector-transfected cells. The A-to-B transport of BAC C8 and C10 was negligible in both vector- and transporter-transfected cells, with BAC levels in the receiver chamber below our LC-MS/MS limit of quantification. The calculated B-to-A P_{app} of BAC C8 was 17.9 ± 0.6 × 10^{-6} cm/s and of C10 was 13.7 ± 1.0 × 10^{-6} cm/s in hOCT2/hMATE1-transfected cells, which are respectively 4- and 1.5-fold higher than the B-to-A P_{app} in vector cells (Fig. 8, C and D). These results suggest that hOCT2 and hMATE1 in the human kidney can facilitate tubular secretion of these compounds. In vector-transfected MDCK cells, there was detectable transport of BAC C8 and C10 in the B-to-A direction but not in the A-to-B direction. The reason for this observation is unknown but may be due to the expression of endogenous transporters in MDCK cells, such as the canine OCT2 and/or P-glycoprotein (Shu et al., 2001; Goh et al., 2002).

Intracellular Accumulation of BAC C8 and C10 in hOCT2/hMATE1-Transfected MDCK Cells. At the end of the transport study, the intracellular accumulation of BAC was measured. When BACs were added to the basal chamber, intracellular accumulation in the double-transfected cells was 8.2 and 3.7 times that in vector cells for C8 and C10, respectively (Fig. 9, A and B). This data suggests that hOCT2 facilitates BAC uptake into MDCK cells at a rate significantly higher than their apical efflux rate mediated by hMATE1. Intriguingly, BACs also accumulated when added to the apical chamber in double-transfected cells, with 15- and 5-fold increase for C8 and C10, respectively, in comparison with vector cells (Fig. 9, A and B). These data are surprising, as they suggest that apical hMATE1 could facilitate BAC uptake into the MDCK cells. To further test this hypothesis, we measured intracellular accumulation of apically added BACs in the absence or presence of the classic hMATE inhibitor pyrimethamine. Indeed, in the presence of 10 μM pyrimethamine added apically, the accumulation of BAC C8 and C10 was significantly reduced (Fig. 9, C and D). Together, these findings strongly suggest that hOCT2 and hMATE1 could play an important role in the intrarenal accumulation of BACs in vivo.

Discussion

Due to the widespread use of BACs in cleaning products (e.g., Lysol, Clorox, hand sanitizers, and wipes) and in pharmaceutical and personal care products, the general population is systemically exposed to these compounds. Studies in rodents have shown that BACs can accumulate in several tissues with especially high levels in the kidneys (Kera et al.,

TABLE 2

Kinetic parameters of BAC C8 and BAC C10 uptake by hOCT1–3 and hMATE1/2K

Models were chosen based on examination of Eadie-Hofstee plots. The standard Michaelis-Menten equation (eq. 2) was fitted to the BAC C8 data, whereas a substrate-inhibition model (eq. 3) was fitted to the BAC C10 uptake kinetics. Results are represented as mean ± S.D. of the K_m, V_{max}, and $K_{i,[s]}$ from three independent experiments.

	BAC C8		BAC C10		
Transporter	K_m (μM)	V_{max} (pmol/mg protein/min)	K_m (μM)	V_{max} (pmol/mg protein/min)	$K_{i,[s]}$ (μM)
hOCT1	8.7 ± 2.3	1091 ± 339	6.8 ± 3.8	1480 ± 163	93.1 ± 19.4
hOCT2	10.4 ± 3.9	965 ± 43	19.1 ± 6.8	2673 ± 412	106.5 ± 11.2
hOCT3	18.9 ± 2.4	1716 ± 157	27.4 ± 22.1	2421 ± 1233	37.1 ± 19.3
hMATE1	6.0 ± 0.7	487 ± 206	4.9 ± 1.4	975 ± 49	52.2 ± 16.2
hMATE2K	9.7 ± 4.1	2239 ± 385	19.3 ± 0.3	6102 ± 973	111 ± 27.6

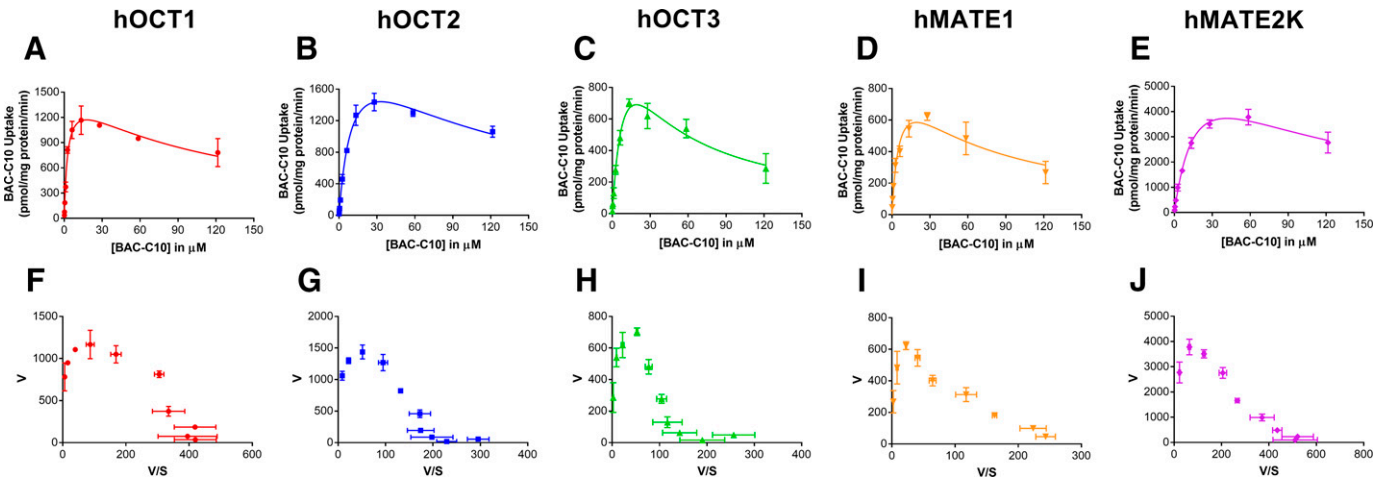

Fig. 7. BAC C10 uptake kinetics by hOCT1–3 and hMATE1/2K. Concentration-dependent uptake was measured in both control and transporter-expressing cell lines at 37°C within the linear phase of uptake (4 minutes for hOCT1–3 and 2 minutes for hMATE1/2K). Transporter-specific uptake was obtained by subtracting the uptake in control cells from the uptake in transporter-expressing cells. (A–E) panels display saturation curves and (F–J) panels show Eadie-Hofstee transformations for the kinetic data. Based on the Eadie-Hofstee plots, a substrate-inhibition kinetic model (eq. 3) was fitted to the data from hOCT1- (A), hOCT2- (B), hOCT3- (C), hMATE1- (D), and hMATE2K- (E) mediated uptake of BAC C10. Concentration-dependent uptake was performed independently three times for each transporter, and results from one representative experiment are shown. Data points represent the mean ± S.D. from one representative experiment in triplicate. The kinetic parameters summarized in Table 2 are the mean ± S.D. of the values from all three independent experiments.

2021). Although the tissue distribution of BACs overlaps significantly with tissue expression of polyspecific organic cation transporters, the roles of these transporters in BAC disposition are currently unknown. In this study, we comprehensively characterized the interaction between BAC C8–C14 with hOCT1–3 and hMATE1/2K transporters as inhibitors or substrates. The role of hOCT2 and hMATE1 in intrarenal accumulation of short-chain BACs was also investigated using an in vitro model of renal secretion. Findings from our study have important implications for improving our understanding of the mechanisms involved in the disposition and systemic toxicology of BACs.

Our studies showed that all investigated BACs (Fig. 1) are potent hOCT and hMATE inhibitors with IC_{50} values in the high nM to low μM range (Fig. 2; Table 1). A previous analysis in 222 human blood samples revealed that the median concentrations of BACs in human serum samples are in the low nanomolar range (Zheng et al., 2021). The calculated IC_{50} values from our study are well above the plasma levels reported for these compounds (Zheng et al., 2021), and although the plasma concentrations of BACs are unlikely to elicit transporter inhibition, the potential of xenobiotic-drug interactions cannot be ruled out due to their extensive tissue accumulation (Xue et al., 2002, 2004; Kera et al., 2021). We did not observe a relationship between BAC chain length and inhibitory potency toward these transporters (Fig. 3). Previous studies analyzing other quaternary ammonium compounds (i.e., n-tetraalkylammonium) have reported a relationship between their inhibitory potency and alkyl chain length (Zhang et al., 1999; Dresser et al., 2002). However, the basic structure of BACs is different from n-tetraalkylammonium compounds. Previous pharmacophore studies on the OCTs showed that inhibitors with a positively charged moiety and a hydrophobic aromatic moiety separated by a distance (i.e., the Ar–N distance) around 1–3 carbon length offer the optimal inhibitor binding to the transporter (Zolk et al., 2009). The presence of the positive charge and the benzyl group at 1 carbon length in all BACs may already satisfy these basic pharmacophore features required for the inhibition of these transporters (Fig. 1). Hence, further increasing the alkyl chain length may not have a significant impact on inhibitor potency.

The alkyl chain length does, however, appear to play a role in the substrate status of these compounds, as our uptake studies revealed that BAC C8 and C10, but not C12 and C14, are good substrates of hOCT1–3 and hMATE1/2K (Fig. 4). Both C8 and C10 are transported by hOCTs and hMATEs with K_m in the low μM range (Table 2). Detailed kinetic analysis showed that although BAC C8 displayed typical Michaelis-Menten kinetics (Fig. 6), C10 demonstrated a more complex substrate-inhibition profile (Fig. 7). hOCTs and hMATEs have been reported to have multiple binding sites (Belzer et al., 2013; Harper and Wright, 2013; Martínez-Guerrero and Wright, 2013; Boxberger et al., 2018). Our results suggest that at higher concentrations, BAC C10 may bind to a second binding region, which may hinder the transport by either an allosteric effect or steric hindrance (Hutzler and Tracy, 2002; Tracy, 2003; Leow and Chan, 2019). Alternatively, BACs are cationic surfactants that could disrupt membrane or cell integrity at higher concentrations, affecting overall cellular accumulation.

The identification of BAC C8 and C10 as substrates of the hOCT1–3 and hMATE1/2K transporters suggests that the polyspecific organic cation transporters could be involved in the tissue-specific disposition of these compounds in humans. The liver is considered a major site of BAC elimination in humans, where these compounds are metabolized via alkyl chain oxidation mediated by the cytochrome P450 enzymes in the CYP4F subfamily and CYP2D6 (Seguin et al., 2019). hOCT1 is highly expressed in the sinusoidal membrane of human hepatocytes, and the identification of BAC C8 and C10 as substrates of hOCT1 suggests that this transporter may mediate the uptake of C8 and C10 into hepatocytes, thus facilitating their metabolism by intracellular enzymes. Additionally, fetal exposure to BACs is of special concern in view that short-chain BACs are potent inhibitors of cholesterol biosynthesis (Herron et al., 2016), which is critical during neurodevelopment (Zhang and Liu, 2015). In fact, rodents exposed to a quaternary ammonium mixture containing BACs have been reported to have decreased fertility and increased incidence of neural tube defects in embryos (Melin et al., 2014, 2016; Hrubec et al., 2017). hOCT3 is highly expressed in the human placenta and could facilitate fetal exposure to organic cation drugs (Lee et al., 2018). It is possible that hOCT3 could facilitate the placental transport of BACs, contributing to the deleterious effects observed in embryonic development.

The hOCT2 and hMATE1/2K transporters have been implicated in the renal elimination and accumulation of many organic cations (Yonezawa and Inui, 2011; Yin and Wang, 2016; López Quiñones et al.,

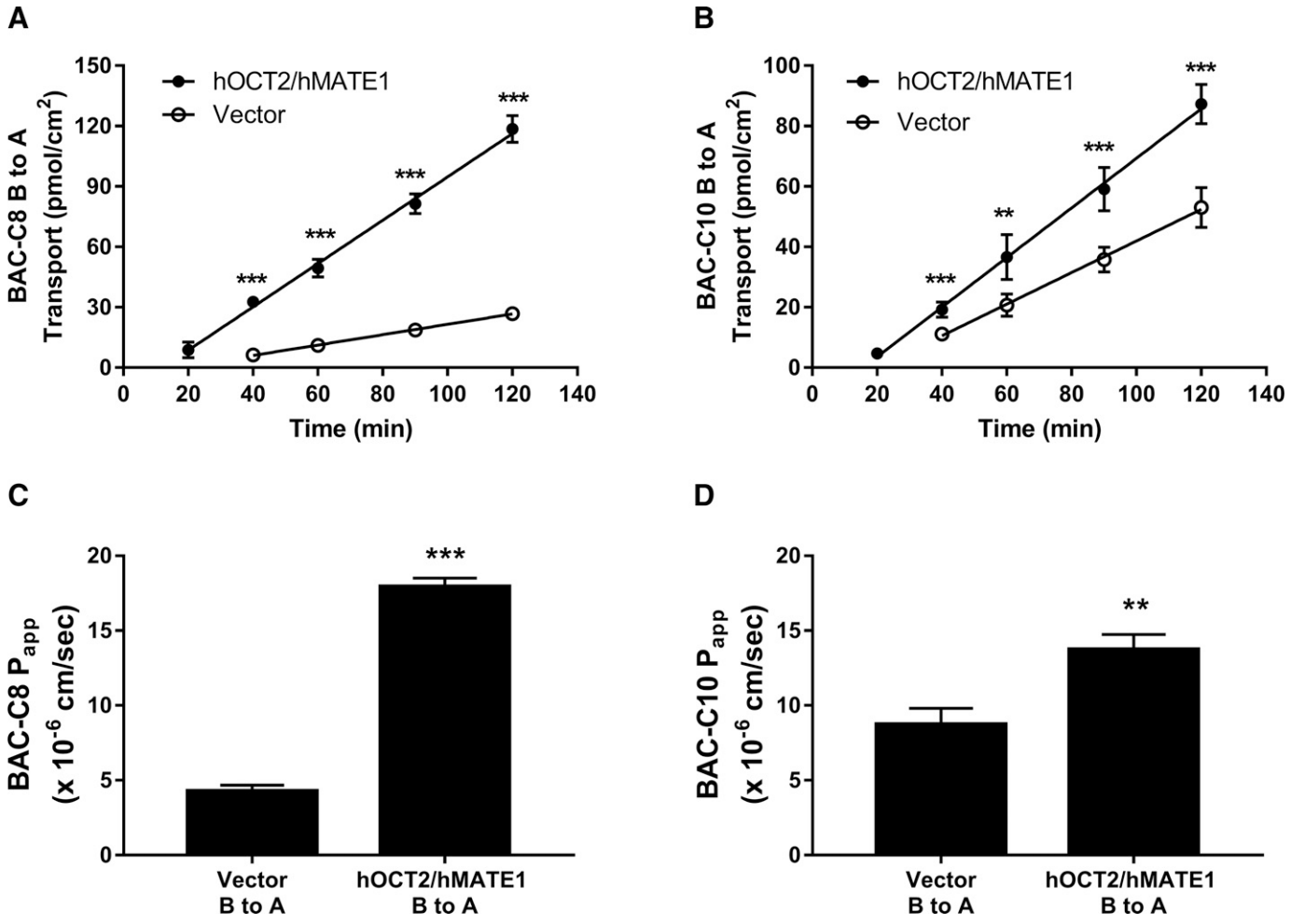

Fig. 8. Transepithelial transport and apparent permeability (P_{app}) of BAC C8 and C10 in vector-transfected and hOCT2/hMATE1 double-transfected MDCK cells. Basolateral to apical (B-to-A) transport of BAC C8 (A) or C10 (B) across vector (open circle) and hOCT2/hMATE1-transfected (closed circle) MDCK monolayers. Apical to basolateral (A-to-B) transport of BAC C8 and C10 were below the limit of quantification and thus are not shown. Transport was initiated by adding KRH buffer containing 1 μM BAC to the basal chamber, and a 100 μl aliquot was collected periodically from the apical chamber and replenished with an equal volume of KRH buffer. BAC C8 and C10 in the aliquots were measured by LC-MS/MS. The pH in the apical and basal chamber was 6.0 and 7.4, respectively. B-to-A P_{app} of BAC C8 (C) and BAC C10 (D) was calculated using eq. 4 described in *Materials and Methods*. Transport and permeability were compared between vector- and OCT2/hMATE1-transfected MDCK cells (**$P < 0.01$; ***$P < 0.001$). Statistical significance was determined by using an unpaired Student's t test with the Bonferroni correction when multiple comparisons were done. Each data point represents the means ± S.D. from three independent experiments (three to six inserts total).

2020). The identification of BAC C8 and C10 as substrates of hOCT2 and hMATE1/2K (Fig. 4) and the results from our transepithelial transport and permeability study (Fig. 8) indicate the involvement of these transporters in renal disposition of these short-chain BACs. Although no parent BACs have been found in human urine samples (Li et al., 2023), it is possible that C8 and C10 are secreted by hOCT2/hMATEs but undergo complete reabsorption in the nephron tubules, similarly to what has been reported for choline (Wright et al., 1992). Importantly, the kidneys have been consistently reported as a major organ for BAC accumulation in various biodistribution studies in rodents. In rats, 30 minutes after a single intravenous dose of BAC mixture (7 mg/kg), the highest level of BAC accumulation was observed in the kidneys, which is ~42-fold higher than serum concentrations (Xue et al., 2002). Similarly, 24 hours after oral administration of BACs (250 mg/kg) to rats, kidney concentrations were 15-fold higher than in blood (Xue et al., 2004). Kera et al. (2021) demonstrated that shorter-chain BACs reached higher concentrations in the kidneys of rats in comparison with longer-chain BACs (C12 > C14 > C16) after intravenous administration of a BAC mixture containing equal amounts of each chain length. In contrast, the lungs and spleen preferentially accumulated longer-chain BACs (C16 > C14 > C12). In the renal proximal tubule cells, hOCT2 and hMATE1 sequentially mediate the uptake and the efflux of substrates, and the interplay between the two transporters can significantly impact intracellular accumulation of the substrates. If efflux is slower than uptake, compounds will accumulate and potentially lead to nephrotoxicity (Yonezawa and Inui, 2011; Yin and Wang, 2016). The higher accumulation observed in the hOCT2/hMATE1-transfected cells when BACs were applied to the basal chamber suggests that hMATE1-mediated efflux is less efficient than OCT2-mediated uptake (Fig. 9).

Interestingly, we also observed a high accumulation of BACs in the hOCT2/hMATE1-transfected cells when BACs were applied to the apical chamber (A-to-B) (Fig. 9). This may suggest that the initial high BAC concentrations in the apical chamber may drive hMATE1 to function as an uptake transporter, allowing BACs to accumulate intracellularly. The contribution of hMATE1 to the apical uptake of C8 and C10 was further corroborated by the inhibitory effect of pyrimethamine—a classic hMATE1 inhibitor—which reduced C8 and C10 accumulation by 40% and 35%, respectively, when added apically (Fig. 9, C and D). This is different from what has been previously observed in our laboratory for other hOCT2/hMATE1 substrates such as atenolol, cimetidine,

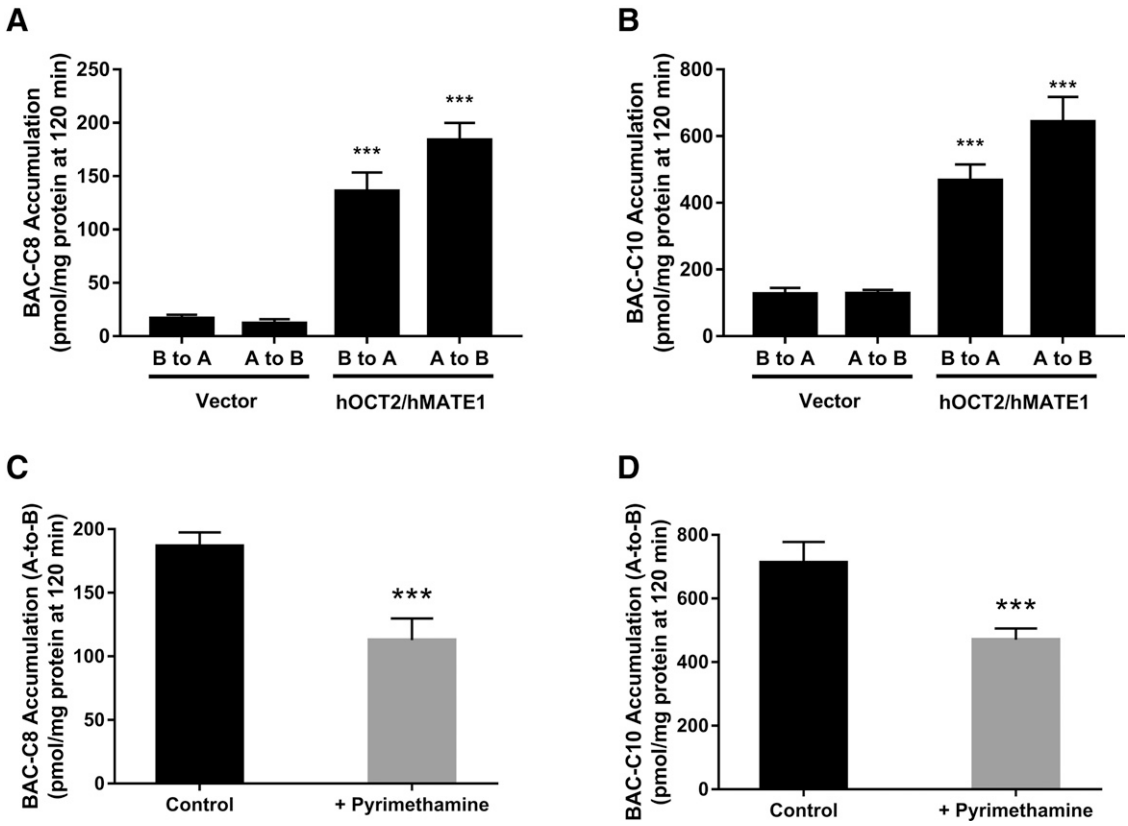

Fig. 9. Intracellular accumulation of BAC C8 and C10 in vector- and hOCT2/hMATE1 double-transfected MDCK cells. At the end of the 120-minute transepithelial transport assay, MDCK cells were lysed and the intracellular accumulation of BAC C8 (A) and C10 (B) was measured by LC-MS/MS and normalized to protein content. Intracellular accumulation of C8 and C10 applied basally or apically in hOCT2/hMATE1-transfected cells were compared with their respective accumulation in vector-transfected MDCK cells (***$P < 0.001$). Additionally, accumulation of C8 (C) and C10 (D) applied apically in hOCT2/hMATE1-transfected cells was measured in the absence (control) or presence of 10 μM pyrimethamine (also applied apically), and values were compared (***$P < 0.001$). Statistical significance was determined by using an unpaired Student's t test with the Bonferroni correction when multiple comparisons were done. Each data point represents the means ± S.D. from data obtained from three independent experiments (three to six inserts total).

and meta-iodobenzylguanidine (Yin et al., 2015, 2016; López Quiñones et al., 2020), for which intracellular accumulation in the A-to-B direction in hOCT2/hMATE1-transfected cells was either comparable or only slightly higher than accumulation in vector-transfected cells. The reason behind this difference is currently unknown. However, in contrast to the other organic cations studied in this double-transfected system, BACs are membrane disruptors, and their addition to the apical side may alter the microenvironment around the apical membrane of cells and dissipate the proton gradient across the membrane, which could potentially impact the directionality of hMATE1-mediated transport. Future studies employing hMATE1 and hOCT2 single-transfected polarized MDCK cells could help further clarify the role of hMATE1 in the renal disposition of short-chain BACs. In conclusion, our transwell study results demonstrate that the expression of hOCT2 and hMATE1 have a substantial impact on the intracellular accumulation of BAC C8 and C10, and thus these transporters may represent a previously unrecognized pathway driving intrarenal accumulation of short-chain BACs in vivo.

In summary, we provide the first evidence that BACs can interact with the polyspecific organic cation transporters both as inhibitors and substrates. Our results showed that BACs C8–C14 are potent inhibitors toward hOCT1–3 and hMATE1/2K and that the shorter-chain BACs (C8 and C10) are excellent substrates of these transporters. Our data suggests that hOCT1 and hOCT3 can be determinants in the distribution of BAC C8 and C10 into tissues such as the liver and placenta, whereas hOCT2 and hMATE1 contribute to renal accumulation of these compounds. Our findings provide new insights on the molecular mechanisms driving the tissue-specific disposition of BACs, which could have implications for understanding and predicting tissue exposure and organ susceptibility to BAC toxicity in humans as a result of chronic environmental exposure.

Acknowledgments

The authors thank the University of Washington Mass Spectrometry Center, especially Dale Whittington and James Movius, for their help and insights in mass spectrometry.

Data Availability

Data generated and analyzed in this study are available upon request from the corresponding author.

Authorship Contributions

Participated in research design: Vieira, Seguin, Xu, Wang.

Conducted experiments: Vieira, Seguin.

Performed data analysis: Vieira, Wang.

Wrote or contributed to the writing of the manuscript: Vieira, Seguin, Xu, Wang.

References

Arnold WA, Blum A, Branyan J, Bruton TA, Carignan CC, Cortopassi G, Datta S, DeWitt J, Doherty A-C, Halden RU, et al. (2023) Quaternary ammonium compounds: a chemical class of emerging concern. *Environ Sci Technol* **57**:7645–7665.

Belzer M, Morales M, Jagadish B, Mash EA, and Wright SH (2013) Substrate-dependent ligand inhibition of the human organic cation transporter OCT2. *J Pharmacol Exp Ther* **346**:300–310.

Boxberger KH, Hagenbuch B, and Lampe JN (2018) Ligand-dependent modulation of hOCT1 transport reveals discrete ligand binding sites within the substrate translocation channel. *Biochem Pharmacol* **156**:371–384.

Brouwer KLR, Keppler D, Hoffmaster KA, Bow DAJ, Cheng Y, Lai Y, Palm JE, Stieger B, and Evers R; International Transporter Consortium (2013) In vitro methods to support transporter evaluation in drug discovery and development. *Clin Pharmacol Ther* **94**:95–112.

Dresser MJ, Xiao G, Leabman MK, Gray AT, and Giacomini KM (2002) Interactions of n-tetraalkylammonium compounds and biguanides with a human renal organic cation transporter (hOCT2). *Pharm Res* **19**:1244–1247.

Duan H and Wang J (2010) Selective transport of monoamine neurotransmitters by human plasma membrane monoamine transporter and organic cation transporter 3. *J Pharmacol Exp Ther* **335**:743–753.

Giacomini KM, Huang S-M, Tweedie DJ, Benet LZ, Brouwer KLR, Chu X, Dahlin A, Evers R, Fischer V, Hillgren KM, et al.; International Transporter Consortium (2010) Membrane transporters in drug development. *Nat Rev Drug Discov* **9**:215–236.

Goh L-B, Spears KJ, Yao D, Ayrton A, Morgan P, Roland Wolf C, and Friedberg T (2002) Endogenous drug transporters in in vitro and in vivo models for the prediction of drug disposition in man. *Biochem Pharmacol* **64**:1569–1578.

Harper JN and Wright SH (2013) Multiple mechanisms of ligand interaction with the human organic cation transporter, OCT2. *Am J Physiol Renal Physiol* **304**:F56–F67.

Herman JR and Bass P (1989) Enteric neuronal ablation: structure-activity relationship in a series of alkyldimethylbenzylammonium chlorides. *Fundam Appl Toxicol* **13**:576–584.

Herron J, Reese RC, Tallman KA, Narayanaswamy R, Porter NA, and Xu L (2016) Identification of environmental quaternary ammonium compounds as direct inhibitors of cholesterol biosynthesis. *Toxicol Sci* **151**:261–270.

Herron JM, Hines KM, Tomita H, Seguin RP, Cui JY, and Xu L (2019) Multiomics investigation reveals benzalkonium chloride disinfectants alter sterol and lipid homeostasis in the mouse neonatal brain. *Toxicol Sci* **171**:32–45.

Herron JM, Tomita H, White CC, Kavanagh TJ, and Xu L (2021) Benzalkonium chloride disinfectants induce apoptosis, inhibit proliferation, and activate the integrated stress response in a 3-D *in vitro* model of neurodevelopment. *Chem Res Toxicol* **34**:1265–1274.

Hitosugi M, Maruyama K, and Takatsu A (1998) A case of fatal benzalkonium chloride poisoning. *Int J Legal Med* **111**:265–266.

Hrubec TC, Melin VE, Shea CS, Ferguson EE, Garofola C, Repine CM, Chapman TW, Patel HR, Razvi RM, Sugrue JE, et al. (2017) Ambient and dosed exposure to quaternary ammonium disinfectants causes neural tube defects in rodents. *Birth Defects Res* **109**:1166–1178.

Hrubec TC, Seguin RP, Xu L, Cortopassi GA, Datta S, Hanlon AL, Lozano AJ, McDonald VA, Healy CA, Anderson TC, et al. (2021) Altered toxicological endpoints in humans from common quaternary ammonium compound disinfectant exposure. *Toxicol Rep* **8**:646–656.

Hutzler JM and Tracy TS (2002) Atypical kinetic profiles in drug metabolism reactions. *Drug Metab Dispos* **30**:355–362.

Kera H, Fuke C, Usumoto Y, Nasu A, Maeda K, Mukai M, Sato W, Tanabe M, Kuninaka H, and Ihama Y (2021) Kinetics and distribution of benzalkonium compounds with different alkyl chain length following intravenous administration in rats. *Leg Med (Tokyo)* **48**:101821.

Koepsell H (2020) Organic cation transporters in health and disease. *Pharmacol Rev* **72**:253–319.

Lee N, Hebert MF, Wagner DJ, Easterling TR, Liang CJ, Rice K, and Wang J (2018) Organic cation transporter 3 facilitates fetal exposure to metformin during pregnancy. *Mol Pharmacol* **94**:1125–1131.

Leow JWH and Chan ECY (2019) Atypical Michaelis-Menten kinetics in cytochrome P450 enzymes: a focus on substrate inhibition. *Biochem Pharmacol* **169**:113615.

Li Z-M, Lakuleswaran M, and Kannan K (2023) LC-MS/MS methods for the determination of 30 quaternary ammonium compounds including benzalkonium and paraquat in human serum and urine. *J Chromatogr B Analyt Technol Biomed Life Sci* **1214**:123562.

Liang X and Giacomini KM (2017) Transporters involved in metformin pharmacokinetics and treatment response. *J Pharm Sci* **106**:2245–2250.

López Quiñones AJ, Wagner DJ, and Wang J (2020) Characterization of meta-iodobenzylguanidine (mIBG) transport by polyspecific organic cation transporters: Implication for mIBG therapy. *Mol Pharmacol* **98**:109–119.

Martínez-Guerrero LJ and Wright SH (2013) Substrate-dependent inhibition of human MATE1 by cationic ionic liquids. *J Pharmacol Exp Ther* **346**:495–503.

Melin VE, Melin TE, Dessify BJ, Nguyen CT, Shea CS, and Hrubec TC (2016) Quaternary ammonium disinfectants cause subfertility in mice by targeting both male and female reproductive processes. *Reprod Toxicol* **59**:159–166.

Melin VE, Potineni H, Hunt P, Griswold J, Siems B, Werre SR, and Hrubec TC (2014) Exposure to common quaternary ammonium disinfectants decreases fertility in mice. *Reprod Toxicol* **50**:163–170.

Müller F, König J, Glaeser H, Schmidt I, Zolk O, Fromm MF, and Maas R (2011) Molecular mechanism of renal tubular secretion of the antimalarial drug chloroquine. *Antimicrob Agents Chemother* **55**:3091–3098.

Nałecz-Jawecki G, Grabińska-Sota E, and Narkiewicz P (2003) The toxicity of cationic surfactants in four bioassays. *Ecotoxicol Environ Saf* **54**:87–91.

Pereira BMP and Tagkopoulos I (2019) Benzalkonium chlorides: uses, regulatory status, and microbial resistance. *Appl Environ Microbiol* **85**:e00377-19.

Rowland M and Tozer TN (2010) *Clinical Pharmacokinetics and Pharmacodynamics: Concepts and Applications*, 4th ed. LWW, Baltimore, MD.

Sala-Rabanal M, Li DC, Dake GR, Kurata HT, Inyushin M, Skatchkov SN, and Nichols CG (2013) Polyamine transport by the polyspecific organic cation transporters OCT1, OCT2, and OCT3. *Mol Pharm* **10**:1450–1458.

Sarkar J, Chaudhary S, Namavari A, Ozturk O, Chang J-H, Yco L, Sonawane S, Khanolkar V, Hallak J, and Jain S (2012) Corneal neurotoxicity due to topical benzalkonium chloride. *Invest Ophthalmol Vis Sci* **53**:1792–1802.

Seguin RP, Herron JM, Lopez VA, Dempsey JL, and Xu L (2019) Metabolism of benzalkonium chlorides by human hepatic cytochromes P450. *Chem Res Toxicol* **32**:2466–2478.

Shu Y, Bello CL, Mangravite LM, Feng B, and Giacomini KM (2001) Functional characteristics and steroid hormone-mediated regulation of an organic cation transporter in Madin-Darby canine kidney cells. *J Pharmacol Exp Ther* **299**:392–398.

Tambuzzi S, Gentile G, Andreola S, Migliorini AS, and Zoja R (2022) Visceral microscopic pattern from suicidal ingestion of professional Lysoform® with delayed death. *Acad Forensic Pathol* **12**:118–125.

Tanihara Y, Masuda S, Sato T, Katsura T, Ogawa O, and Inui K (2007) Substrate specificity of MATE1 and MATE2-K, human multidrug and toxin extrusions/H(+)-organic cation antiporters. *Biochem Pharmacol* **74**:359–371.

Tracy TS (2003) Atypical enzyme kinetics: their effect on in vitro-in vivo pharmacokinetic predictions and drug interactions. *Curr Drug Metab* **4**:341–346.

Tsuda M, Terada T, Ueba M, Sato T, Masuda S, Katsura T, and Inui K (2009) Involvement of human multidrug and toxin extrusion 1 in the drug interaction between cimetidine and metformin in renal epithelial cells. *J Pharmacol Exp Ther* **329**:185–191.

US FDA (2015) Safety and effectiveness of health care antiseptics; topical antimicrobial drug products for over-the-counter human use; proposed amendment of the tentative final monograph; reopening of administrative record. *Fed Regist* **80**:25166–25205.

US FDA (2016) Safety and effectiveness of consumer antiseptics; topical antimicrobial drug products for over-the-counter human use; proposed amendment of the tentative final monograph; reopening of administrative record. *Fed Regist* **81**:42912–42937.

van Berkel M and de Wolff FA (1988) Survival after acute benzalkonium chloride poisoning. *Hum Toxicol* **7**:191–193.

Wagner DJ, Hu T, and Wang J (2016) Polyspecific organic cation transporters and their impact on drug intracellular levels and pharmacodynamics. *Pharmacol Res* **111**:237–246.

Wright SH, Wunz TM, and Wunz TP (1992) A choline transporter in renal brush-border membrane vesicles: energetics and structural specificity. *J Membr Biol* **126**:51–65.

Xue Y, Hieda Y, Kimura K, Nishiyama T, and Adachi T (2002) Sensitive determination of benzalkonium chloride in blood and tissues using high-performance liquid chromatography with solid-phase extraction. *Leg Med (Tokyo)* **4**:232–238.

Xue Y, Hieda Y, Saito Y, Nomura T, Fujihara J, Takayama K, Kimura K, and Takeshita H (2004) Distribution and disposition of benzalkonium chloride following various routes of administration in rats. *Toxicol Lett* **148**:113–123.

Yin J, Duan H, Shirasaka Y, Prasad B, and Wang J (2015) Atenolol renal secretion is mediated by human organic cation transporter 2 and multidrug and toxin extrusion proteins. *Drug Metab Dispos* **43**:1872–1881.

Yin J, Duan H, and Wang J (2016) Impact of substrate-dependent inhibition on renal organic cation transporters hOCT2 and hMATE1/2-K-mediated drug transport and intracellular accumulation. *J Pharmacol Exp Ther* **359**:401–410.

Yin J and Wang J (2016) Renal drug transporters and their significance in drug-drug interactions. *Acta Pharm Sin B* **6**:363–373.

Yonezawa A and Inui K (2011) Organic cation transporter OCT/SLC22A and H(+)/organic cation antiporter MATE/SLC47A are key molecules for nephrotoxicity of platinum agents. *Biochem Pharmacol* **81**:563–568.

Zhang J and Liu Q (2015) Cholesterol metabolism and homeostasis in the brain. *Protein Cell* **6**:254–264.

Zhang L, Gorset W, Dresser MJ, and Giacomini KM (1999) The interaction of n-tetraalkylammonium compounds with a human organic cation transporter, hOCT1. *J Pharmacol Exp Ther* **288**:1192–1198.

Zheng G, Webster TF, and Salamova A (2021) Quaternary ammonium compounds: bioaccumulation potentials in humans and levels in blood before and during the Covid-19 pandemic. *Environ Sci Technol* **55**:14689–14698.

Zolk O, Solbach TF, König J, and Fromm MF (2009) Structural determinants of inhibitor interaction with the human organic cation transporter OCT2 (SLC22A2). *Naunyn Schmiedebergs Arch Pharmacol* **379**:337–348.

Address correspondence to: Dr. Joanne Wang, University of Washington, Department of Pharmaceutics, H272 Health Sciences Building, PO Box 357610, Seattle, WA 98195. E-mail: jowang@uw.edu; or Dr. Libin Xu, University of Washington, Department of Environmental and Occupational Health Sciences and Department of Medicinal Chemistry, H172 Health Sciences Building, PO Box 357610, Seattle, WA 98195. E-mail: libinxu@uw.edu